MR Spectroscopy without Water Suppression using the Gradient Impulse Response Function

James B. Bacon[1], Peter Jezzard[1], William T. Clarke[1]

[1]Oxford Centre for Integrative Neuroimaging, FMRIB, Nuffield Department of Clinical Neurosciences, University of Oxford

Keywords: MR Spectroscopy, Single Voxel Spectroscopy, Gradient Impulse Response Function, Water Suppression, System Imperfections: Measurement & Correction

Corresponding Author: William T. Clarke, william.clarke@ndcn.ox.ac.uk,
FMRIB Centre, John Radcliffe Hospital, Headington, Oxford, OX3 9DU, United Kingdom

Word Count: 2961

Abstract

Purpose: Non-water-suppressed proton spectroscopy, ^{1}H-MRS, is desirable, as retaining the strong water resonance can facilitate automated online data corrections and enable internal concentration referencing. Additionally, removal of the water suppression module can reduce minimum TR and sequence SAR. However, water suppression is typically considered essential due to eddy current-induced antisymmetric sidebands on the water resonance that distort the spectral baseline and obscure the metabolite signals.

Theory and Methods: The Gradient Impulse Response Function (GIRF) was used to predict time-dependent magnetic field perturbations during the FID that give rise to artefactual sidebands. The GIRF was measured in a one-time calibration, independent of spectroscopy acquisitions, enabling post-processing correction of the sidebands without sequence modification or specialized hardware. GIRF-corrected non-water-suppressed single-voxel-spectroscopy (SVS) was compared to otherwise identical water-suppressed acquisitions in eight participants, at 3T, using semi-LASER and MEGA-PRESS sequences.

Results: Across all participants, GIRF correction reduced sideband amplitudes to levels comparable to the spectral baseline, enabling recovery of the underlying metabolite signals. Systematic increases in quantified metabolite concentrations were observed relative to water-suppressed acquisitions, consistent with water-suppression-induced magnetization transfer effects. Total creatine exhibited the largest increase, with enhancement ratios of 1.069±0.039 for MEGA-PRESS and 1.535±0.160 for semi-LASER acquisitions.

Conclusion: Gradient-induced artefactual sidebands in non-water-suppressed MR spectroscopy can be effectively corrected using the GIRF to predict time-dependent magnetic field perturbations during the FID. While demonstrated here for two SVS sequences and voxel positions at 3T, the approach is, in principle, extendable to other SVS sequences and field strengths, subject to appropriate system calibration.

Introduction

Water suppression in proton spectroscopy, ^{1}H-MRS, is generally considered essential, as antisymmetric sidebands on the water resonance strongly distort the spectral baseline and obscure the metabolite signals. These antisymmetric sidebands arise from time-dependent field perturbations during the FID, which are themselves caused by eddy currents and mechanical vibrations induced in the MRI hardware[1–3] during gradient switching. However, acquiring ^{1}H-MRS data without water suppression offers several potential advantages.

First, obviating the need for RF pulses required to suppress the water resonance decreases the sequence SAR[4], shortens the minimum TR, and minimizes changes in the observed amplitude of metabolite resonances through magnetization transfer effects[5–7]. Second, retaining the strong water signal enables online prospective shim, frequency, and motion correction[8], and automated retrospective automated phase and frequency corrections, even in low SNR conditions. Third, the water signal may serve as an internal concentration reference for metabolite quantification[9], and may additionally be used to track BOLD (line-narrowing) effects in functional MRS[10]. Finally, downfield labile peaks may remain detectable without water suppression[11]. Accordingly, several previous studies have sought to compensate for these artefactual sidebands without using water suppression[12].

Nixon *et al*.[1] proposed a theoretical model in which the spectral sidebands arise from exponentially damped sinusoidal phase modulations of the NMR signal. These modulations originate from Lorentz force-induced deformations of the gradient coil windings, leading to oscillations, thought to be mechanical[2], that perturb the static B_0 field. Such frequency-dependent modulations are not addressed by vendor-implemented pre-emphasis schemes, which model the eddy currents solely as sums of exponential decays[13,14]. Using a model comprising 40-50 frequency-dependent terms, Nixon *et al*. demonstrated compensation of the artefactual sidebands at isocenter through the application of a predetermined correction waveform stored in local memory. However, their analysis indicated that complete suppression of sidebands away from isocenter would require damped sinusoidal pre-emphasis of the linear gradients, which could not be realized within their available hardware constraints.

Alternatively, two-scan approaches[2,15–17] exploit the fact that the sideband appearance is a function of the applied gradients and the central peak state. By acquiring two scans with opposite gradient polarity or frequency-selective inversion (excluding the central water peak, known as metabolite cycling) and summing or subtracting the pair, the sidebands can be cancelled. However, these approaches typically suffer from increased acquisition time, increased sequence complexity, increased SAR, and increased sensitivity to participant motion, B_1^+ inhomogeneity, and B_0 instability. Further alternatives attempt to reduce sidebands through sequence optimization and post processing[4,18]; however, these methods do not readily generalize across sequences, protocols and scanners, and typically only achieve a reduction rather than complete elimination of the sidebands.

Other than the approach proposed by Nixon *et al*.[1], which was limited by hardware constraints, no previous method has explicitly sought to characterize and compensate for the system imperfections responsible for the gradient-induced sidebands in non-water-suppressed spectroscopy. Consequently, irrespective of their individual limitations, existing approaches are not directly applicable to MRS sequences used in routine practice without substantial modification. As a result, water suppression[19–21] remains the common practice, with Klose's method[22] employed to address sidebands on the metabolite resonances themselves.

To address these limitations and to introduce a generalized method for water-unsuppressed ^{1}H-MRS, this study proposes an approach in which gradient-induced field perturbations are characterized using the Gradient Impulse Response Function (GIRF)[23]. The GIRF provides an accurate system-level model of the gradient response, capturing eddy current-related and other dynamic field effects. For a sequence with a known gradient sequence, this enables a post-processing prediction of the B_0 perturbation during the FID and subsequent correction of the resulting artefactual sidebands. The GIRF is acquired in a one-time calibration scan, independent of spectroscopy acquisition, enabling non-water-suppressed single-voxel spectroscopy (SVS) that is generalizable across sequences, protocols and spatial locations, without the need for additional hardware.

Theory

Introduced by Vannesjo *et al.*[23] the GIRF provides an accurate system-level description of gradient-induced imperfections in MR imaging. To paraphrase the aforementioned reference, for a linear time-invariant system, the relationship between the input to the system, $i(t)$, representing the requested gradient waveform, and the corresponding output, $o(t)$, representing the actual gradient-induced magnetic field, is fully characterized by the impulse response, $h(t)$, as described by[24]:

$$o(t) = \int_{-\infty}^{\infty} i(\tau) \cdot h(t-\tau)\, d\tau \Leftrightarrow O(\omega) = I(\omega) \cdot H(\omega) \tag{1}$$

where t and ω are time and angular frequency and $O(\omega)$, $I(\omega)$ and $H(\omega)$ are the Fourier transforms of $o(t)$, $i(t)$ and $h(t)$ respectively[23].

Eddy currents and the associated mechanical vibrations, which are responsible for the artefactual sidebands observed in spectroscopy, can be well approximated as linear mechanisms[1,25,26]. Consequently, their effects contribute to and can be characterized by the GIRF in the frequency domain, $H(\omega)$. In practice, once the GIRF has been measured, it can be used to simulate the actual gradient-induced magnetic fields generated during an MR pulse sequence, including during the readout[27], as shown in Figure 1. This enables an accurate prediction of the resulting frequency-dependent field perturbations during the FID and subsequent post-processing compensation of the associated sidebands.

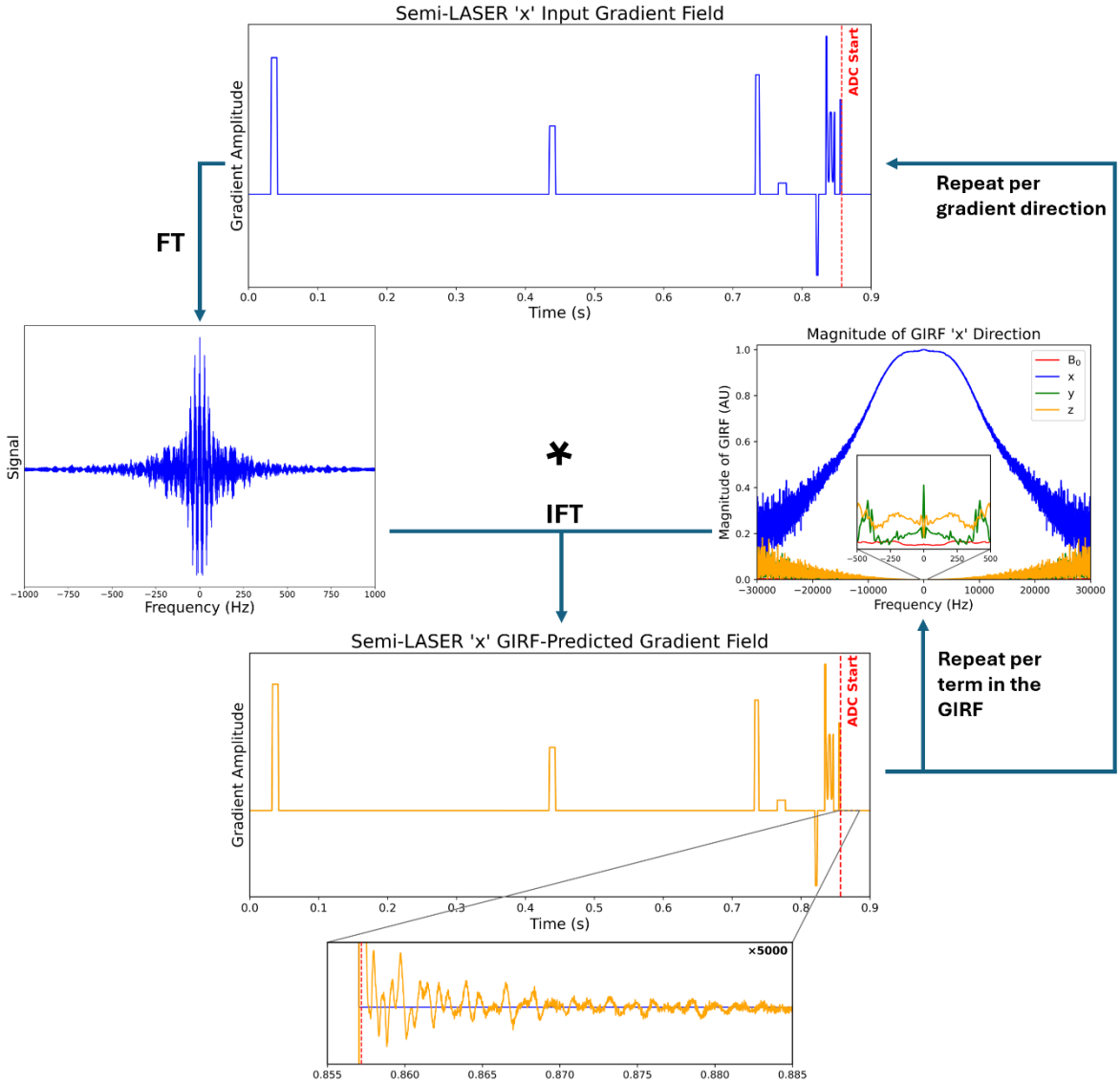

Figure 1: Simulation of the actual gradient-induced magnetic fields during a semi-LASER sequence using the GIRF. The requested x-directed gradient waveform is multiplied by the self-response term of the GIRF in the frequency domain. Inverse Fourier transform back to the time domain allows prediction of the actual gradient field and the resulting frequency-dependent field perturbations during the ADC readout. For a complete prediction of the output field, this process is repeated for each term in the GIRF (up to first-order spherical harmonics in this case) and for each gradient input direction.

Methods

The GIRF was measured on a 3T Prisma scanner (Siemens Healthineers, Erlangen, Germany) in a one-time calibration scan using an open-source, phantom-based method[28], previously optimized for high spectral resolution[29]. The measurement employed an optimized thin-

slice approach in which 18 positive and 18 negative triangular input gradients were applied at four offset thin slices within the phantom[30,31]. An 11 × 11 elliptical 2D phase encoding scheme[32] was used within each slice to assess in-plane spatial variation of the GIRF, and terms up to the first-order spherical harmonics were included in the subsequent sideband correction. The B_0-cross terms and self-response terms used in the correction had a spectral resolution of 5 Hz, whereas the first order-cross terms were represented at a reduced spectral resolution of 10 Hz due to the lower SNR available to these components. The full implementation of this method is available at https://github.com/jbbacon/GIRF_PE_Python.

A $NiCl_2$-doped water phantom (deionized H_2O, $NiCl_2$: 5.5 mM, NaCl: 30.0 mM) was used for GIRF calibration, as it produces a single resonance peak, thereby avoiding contamination of the B_0-cross term with additional resonances that would otherwise propagate into the corrected SVS spectra. The phantom was spherical, using a SPARK casing (Gold Standard Phantoms, Sheffield, UK) with a small diameter (11 cm) to minimize B_1^+ inhomogeneity.

In separate sessions, on eight different days (all different to the day of GIRF calibration), in vivo SVS was performed on the same scanner in eight healthy participants (32.1±12.3 years, 71.6±14.7 kg, 5 male). Data was acquired under a technical development protocol approved by local ethics and institutional committees. Measurements were also acquired in a uniform, metabolite-containing SPECTRE phantom (Gold Standard Phantoms, Sheffield UK).

A vendor-harmonized semi-LASER sequence from the CMRR spectroscopy package[33] (20 mm isotropic voxel; TE/TR: 30/5000 ms; bandwidth: 6000 Hz; GOIA-WURST pulses) was used in the motor cortex, and a MEGA-PRESS sequence, locally modified from the CMRR spectroscopy package[34], (25 × 20 × 25 mm^3 voxel; TE/TR: 68/1500 ms; bandwidth: 4000 Hz) was used in the early-visual cortex (oblique orientation). Non-water suppressed spectra were acquired with VAPOR[19] water suppression disabled, while water-suppressed spectra with VAPOR enabled were acquired as a comparison. Outer-volume suppression (OVS) was enabled in both cases. To assess the potential effects of system heating on the GIRF correction, the non-water-suppressed semi-LASER spectra were reacquired approximately 25 minutes after initial acquisition, and immediately following a 6-minute diffusion tensor imaging sequence (UK Biobank protocol[35]), selected to induce system heating through a high gradient duty cycle.

Eddy current-induced artefactual sidebands were removed by:

1. Simulating the gradient waveforms present in each sequence, using the Siemens POET pulse sequence simulation tool, and extracting them to form the input gradients in latter steps. Simulated protocol parameters were matched to in vivo parameters for each subject.
2. Predicting the achieved gradient fields by multiplying the input gradients by the GIRF in the frequency domain, yielding the magnetic fields occurring throughout the sequence, including during the readout (Figure 1).
3. Computing the accumulated phase coefficient, $k_m(t)$, for each spherical harmonic term by time-integrating the predicted output field, $o_m(t)$, over the readout window up to each time point according to

$$k_m(t) = \gamma \int_{t_s}^{t} o_m(\tau)\ d\tau,\ \ t_s \leq t \leq t_e, \tag{2}$$

   where γ is the proton gyromagnetic ratio, t_s and t_e denote the start and end of the readout period, and m indexes the individual GIRF terms.
4. Calculating the accumulated phase error by multiplying $k_m(t)$ by the spatial dependence of the corresponding spherical harmonic term, evaluated at the voxel center.
5. Correcting the measured signal by subtracting the total accumulated phase error from the phase of the FID at each time point after temporal alignment.

Metabolite concentrations for the GIRF-corrected non-water-suppressed spectra (Figure 2) were quantified using FSL-MRS[36], version 2.4.9. For each participant and acquisition, the water resonance was first modelled individually using a dedicated water basis set with a Voigt lineshape model. The water resonance was fitted over a restricted frequency range (-10 to 4.55 ppm), rather than across the full water peak, to ensure accurate modelling in the region overlapping the metabolite resonances while minimizing interference with the spectral baseline (Figure 3A). The modelled water was subsequently subtracted from the raw data, prior to metabolite quantification. Example spectra, following water removal, are shown in Figure 3 B&C and are provided for each participant in Supporting Information Figure S1.

Prior to spectral fitting, standard preprocessing steps were applied, including RF coil combination, retrospective correction of frequency and phase drifts, and signal averaging[37].

For the water-suppressed reference data only, additional preprocessing included correction of eddy current effects using the Klose method[22] and removal of residual water. Automated phasing was performed using the NAA resonance for the water suppressed data and using the water resonance for the non-water-suppressed data. Following GIRF correction and water removal, the non-water-suppressed data were subsequently realigned relative to the water-suppressed reference.

The remaining metabolite signals were fitted using sequence- and echo-time-specific metabolite basis sets simulated using FSL-MRS. Each basis set comprised 18 metabolites and an appropriate mobile macromolecule spectrum (semi-LASER: empirically measured using a metabolite-nulled acquisition; MEGA-PRESS: parameterized based on published literature[38]). In addition, a lipid resonance was included for the semi-LASER acquisition of one participant exhibiting substantial lipid contamination. For the MEGA-PRESS dataset, only the unedited 'off' spectra were fitted, as the water-resonance, sidebands, and GIRF correction are cancelled out during the editing process[39]; i.e., high quality MEGA-PRESS data can be acquired without water suppression or sideband removal . Spectral fitting was performed using a Voigt lineshape model with a moderate penalized spline baseline[40] over a frequency range of 0.2-4.2 ppm.

The full pipeline including preprocessing, GIRF correction and spectral fitting is made available with example data at https://github.com/jbbacon/NWS_Spectroscopy. All processing was performed retrospectively offline in Python.

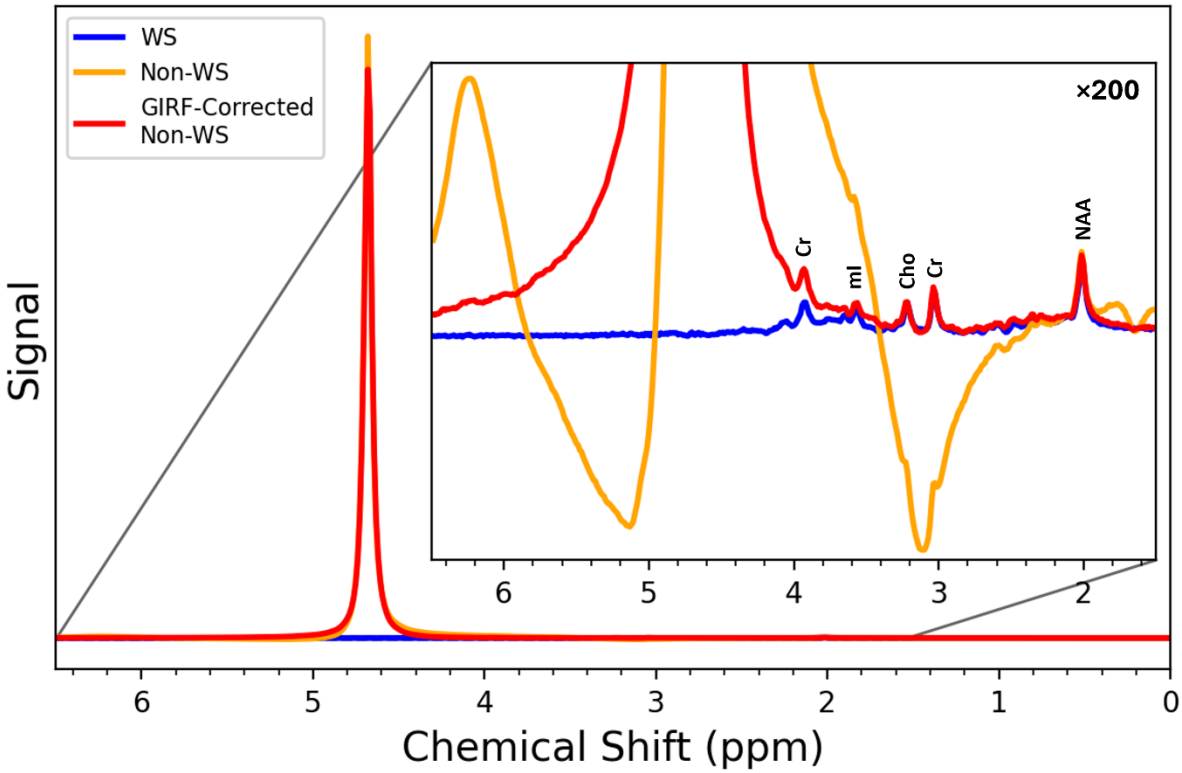

Figure 2: The GIRF-corrected non-suppressed spectrum (GIRF-Corrected Non-WS, red) shown alongside the uncorrected non-water-suppressed spectrum (Non-WS, orange) and the water-suppressed reference spectrum (WS, blue) for a representative participant acquired using the semi-LASER acquisition. The GIRF correction retains the strong water resonance while eliminating the artefactual antisymmetric sidebands, yielding a spectrum comparable to the water-suppressed reference. Key metabolite resonances are labelled in the magnified (×200) view. Spectra from all subjects and sequences are shown in Supporting Information Figure S1.

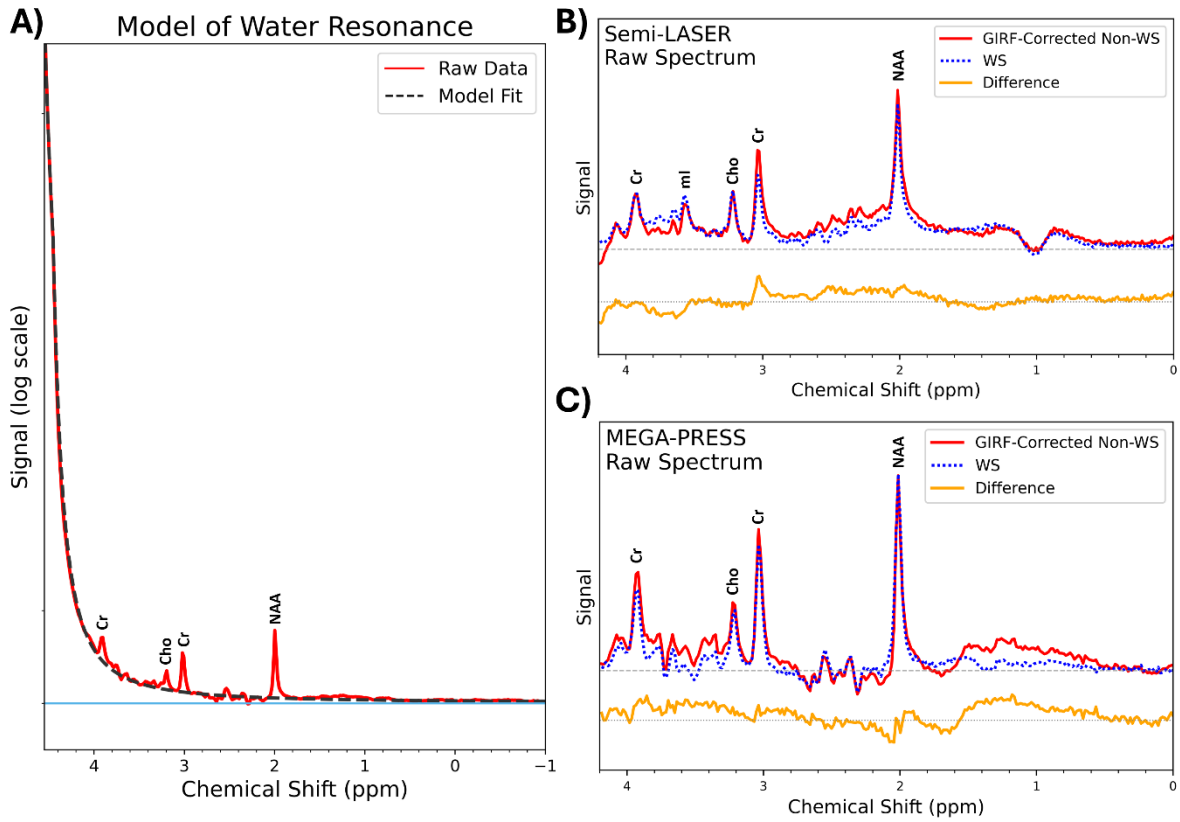

Figure 3: A) Modelling of the water resonance in an example MEGA-PRESS 'off' spectrum (editing pulses at control position[39]). The water signal is fit over a restricted frequency range without the inclusion of a baseline. B, C) Semi-LASER and MEGA-PRESS 'off' spectra for an example participant following subtraction of the modelled water signal from the raw data. The corresponding water-suppressed reference spectra are shown alongside the difference relative to the GIRF-corrected non-water-suppressed spectra. For visual clarity, the difference spectra are vertically offset.

Results

Representative examples of the fitted metabolite spectra are shown in Figure 4, alongside the corresponding water-suppressed reference spectra. Fitted spectra for all participants are provided in the Supporting Information Figure S2, including the semi-LASER spectra reacquired following mild system heating (Figure S3). In each case, the GIRF-corrected non-water-suppressed spectra closely reproduce water-suppressed reference results, except for the creatine resonances at 3.03 and 3.92 ppm, which appear elevated in the GIRF-corrected data. Visually, agreement between the GIRF-corrected and reference-spectra is stronger for the MEGA-PRESS dataset than for the semi-LASER acquisitions.

Figure 5 and Table 1 summarise the ratio of the metabolite concentrations measured with and without water suppression for key metabolites. In the MEGA-PRESS data, there is strong

agreement between the two approaches, except for the expected increase of total creatine which exhibits an enhancement ratio (non-suppressed to suppressed) of 1.069±0.039. The semi-LASER data, however, shows more variability, with significant increases in total NAA, total creatine, myo-inositol, and total choline. Among these, total creatine exhibits the largest increase, with an enhancement ratio of 1.535±0.160. No significant differences were observed in the metabolite ratios for the semi-LASER data acquired before and after system heating.

Figure 6 shows the raw and fitted spectra acquired in the SPECTRE phantom, while Table 2 summarises the ratio of the metabolite concentrations measured with and without water suppression. In contrast to the in vivo results, no visible disagreement was observed between the two approaches, and no significant differences were detected in the metabolite concentrations, other than a minor increase in total choline for the semi-LASER data.

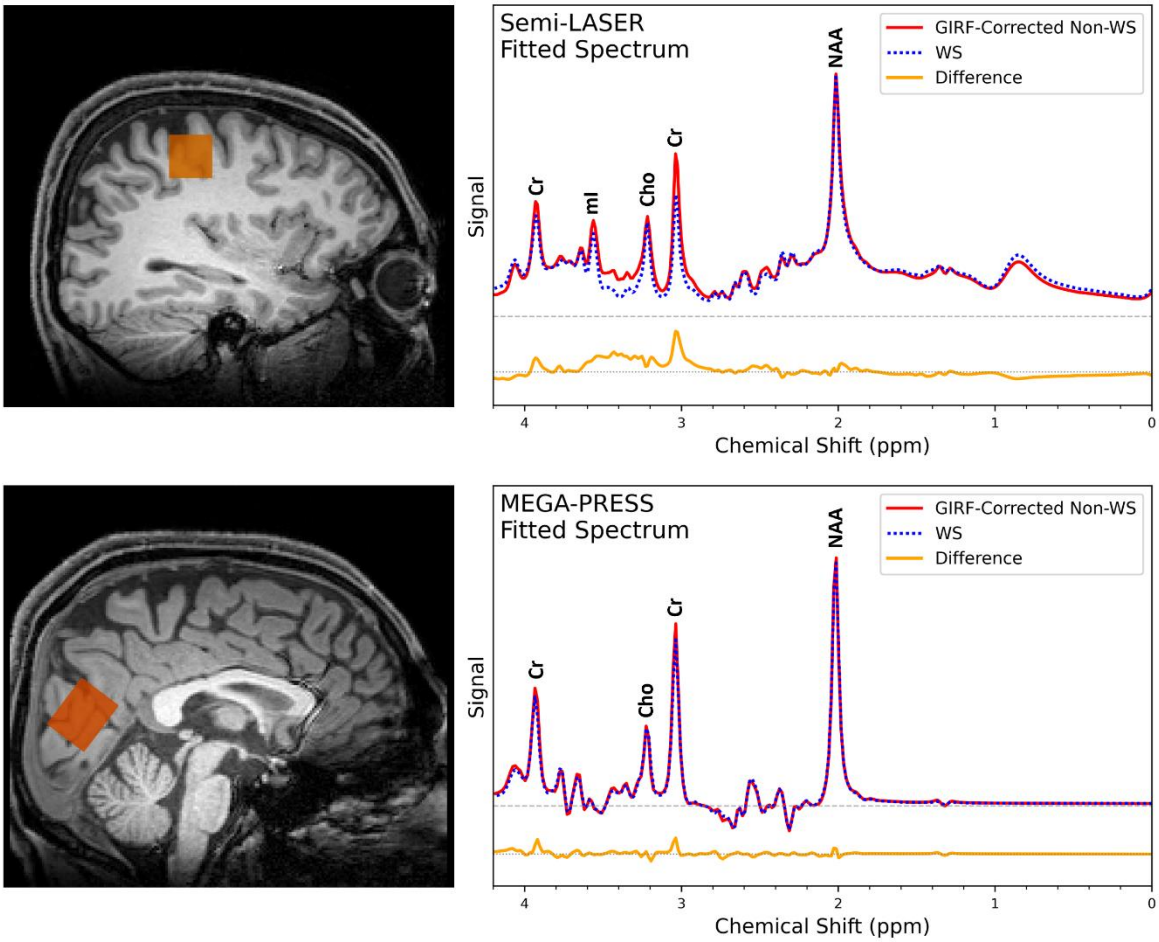

Figure 4: Comparison of the GIRF-corrected non-water-suppressed (red) and water-suppressed (blue) fitted spectra (baseline removed) for a representative participant. The difference spectrum (orange) is vertically offset for clarity. The corresponding voxel

locations are shown on the anatomical images (left). Creatine resonances appear elevated in the GIRF-corrected spectra, with larger differences observed in the semi-LASER acquisition.

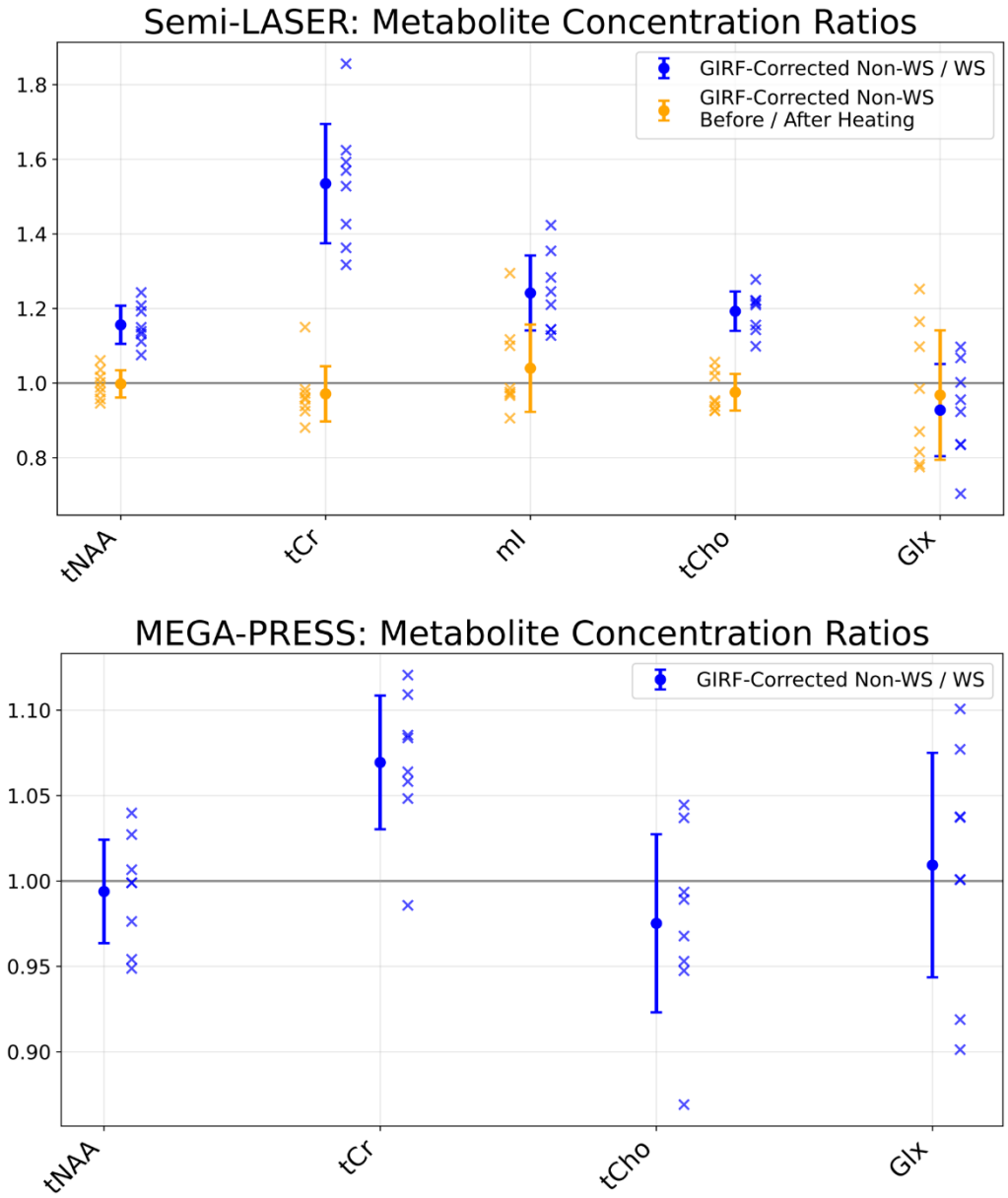

Figure 5: Ratios of key metabolites measured with and without water suppression (blue) and before and after system heating (orange). Top: Semi-LASER data shows strong consistency before and after system heating, but greater variability between water-suppression conditions. Bottom: MEGA-PRESS data shows strong agreement, except for total creatine. *Abbreviations: tNAA, total NAA; tCr, total creatine; mI, myo-inositol; tCho, total choline; Glx, glutamate + glutamine.*

Metabolite	Semi-LASER Non-WS / WS	Semi-LASER Before / After Heating	MEGA-PRESS Non-WS / WS
tNAA	1.156±0.051	0.998±0.037	0.994±0.030
tCr	1.535±0.160	0.971±0.074	1.069±0.039
mI	1.242±0.100	1.040±0.117	-
tCho	1.193±0.053	0.975±0.049	0.975±0.052
Glx	0.927±0.123	0.968±0.174	1.009±0.066

Table 1: Ratios (Mean ± SD, n = 8) of metabolite concentrations measured with and without water-suppression and before and after system heating. Myo-inositol is not quantified for the MEGA-PRESS data due to its low signal in the 'off' spectrum.

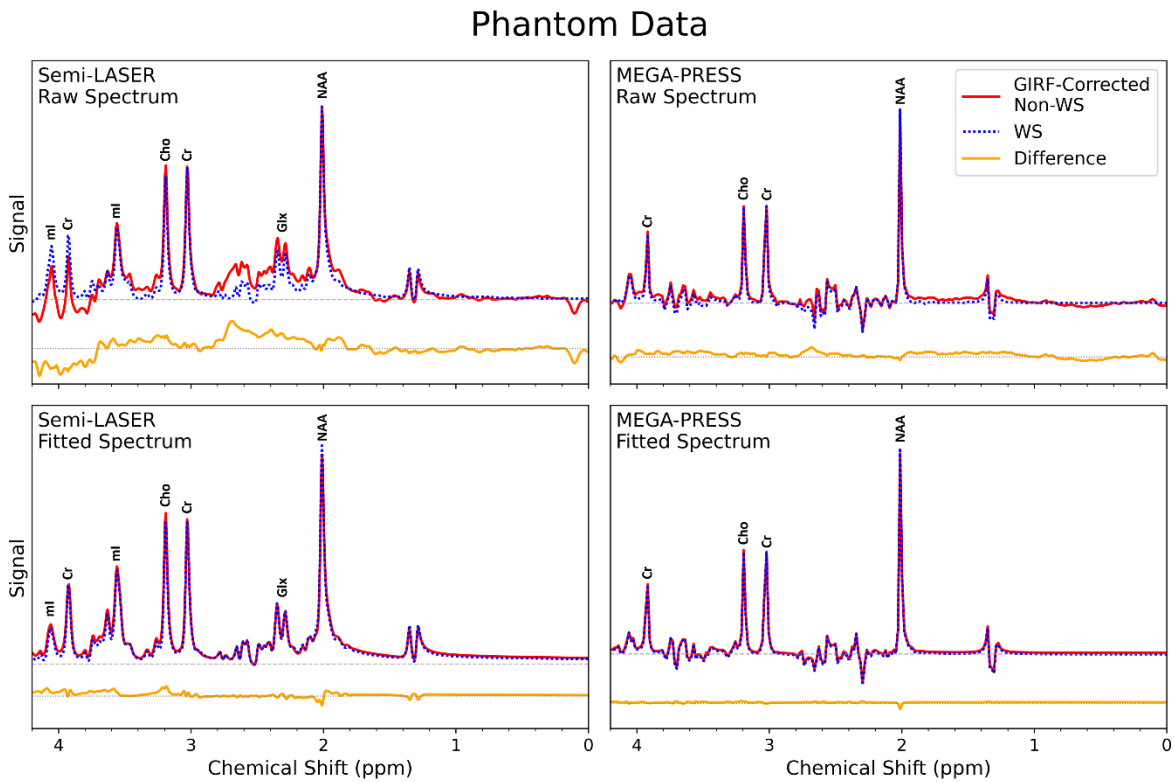

Figure 6: Comparison of the GIRF-corrected non-water-suppressed (red) and water-suppressed (blue) spectra acquired in the SPECTRE phantom. Top row: Raw spectra following water removal show no visible disagreement, aside from minor differences in the spectral baseline and a small residual eddy current at 2.68 ppm. Bottom row: Fitted spectra similarly display only small differences attributable to phase misalignment associated with narrow linewidths. A 6 Hz apodization was applied to all spectra for visualization.

Metabolite	Semi-LASER Non-WS / WS	Semi-LASER Before / After Heating	MEGA-PRESS Non-WS / WS
tNAA	0.994±3.945%	1.004±6.252%	0.968±3.292%
tCr	1.009±4.034%	0.999±6.489%	0.987±3.744%
mI	1.001±4.762%	0.941±7.029%	-
tCho	1.083±4.263%	1.005±6.703%	1.016±4.516%
Glx	0.985±7.343%	0.967±9.745%	0.956±7.954%

Table 2: Ratios (value ± Cramér-Rao Lower Bound (CRLB) (%)) of metabolite concentrations measured with and without water suppression and before and after system heating in the SPECTRE phantom. Myo-inositol is not quantified for the MEGA-PRESS data due to its low concentration in the unedited 'off' spectra.

Discussion

This study demonstrates that gradient-induced artefactual sidebands in non-water-suppressed MR spectroscopy can be effectively corrected by using the GIRF to predict time-dependent B_0 variations during the FID. Across all participants, the application of the GIRF correction reduced the amplitude of the sidebands to levels comparable to the spectral baseline, enabling recovery of the underlying metabolite signals in non-water-suppressed acquisitions.

Although small residual eddy current features were observed in some GIRF-corrected spectra (Figure 6 and S1), these residuals were largely accounted for during spectral fitting and did not significantly affect metabolite quantification. The presence of such residual eddy currents is not unexpected. Given that the GIRF is measured in a separate, one-time calibration, the correction therefore depends on the state of the scanner at the time of the spectroscopy acquisition, which may be altered due to effects such as system heating and drift between sessions.

While the present investigation of the heating effects was not exhaustive, metabolite concentrations remained consistent before and after a high duty cycle diffusion imaging sequence within the same scanning session, indicating that this approach is robust to changing system state within a single session. This consistency also demonstrates the repeatability of the proposed correction when applied to the same participant.

In this study, the B_0-cross term and self-response term of the GIRF, which account for the majority of measured eddy current effects[1], were characterised with a spectral resolution of 5 Hz. This represents a substantial improvement from the spectral resolution used in imaging studies[23,27,30] (≈20 Hz) and is necessary to accurately capture low-frequency field perturbations (<500 Hz) relevant to spectroscopy at 3T. However, increasing spectral resolution by extending the amount of data used to calculate the GIRF reduces the SNR of the measurement, with the GIRF exhibiting progressively lower SNR at higher frequencies. Consequently, correction of the eddy currents in the kilohertz range was incomplete, and inclusion of higher-order GIRF terms was avoided, as these components exhibit substantially lower SNR and would further increase noise propagation into the corrected spectra. For the given measurement approach, we consider it unlikely that the spectral resolution could be further improved without introducing excessive noise into the frequency band relevant for spectroscopy.

Over longer timescales, degradation in gradient performance may also affect correction accuracy. While previous work has demonstrated GIRF stability to be within 0.1% below 10 kHz over a period of three years[27], it is currently unclear how often the GIRF will need to be recalibrated for this application. It is likely that mitigation of small residual eddy currents may be improved by real time monitoring of the output field using a dynamic field camera; however, such hardware remains costly and not widely available in research or clinical settings.

Figure 5 demonstrates systematic increases in several metabolite concentrations measured without water suppression compared to reference spectra acquired with VAPOR enabled. In the MEGA-PRESS data, this effect was observed only for total creatine, whereas the semi-LASER data showed larger and more widespread increases in total NAA, total creatine, myo-inositol, and total choline, with the largest relative increase observed for total creatine. These differences were reproducible across participants and were not influenced by mild system heating, suggesting that they do not arise from residual gradient-induced artefacts alone.

We believe these systematic differences arise due to the water-mediated saturation transfer associated with the use of water suppression. When the water magnetisation is manipulated using schemes such as VAPOR, its state is transferred from the water pool to the metabolite resonances, resulting in an apparent reduction in the measured metabolite concentrations

relative to non-water-suppressed acquisitions[5]. Such effects have been reported in several previous studies, including increases in the metabolite concentrations when off-resonance saturation pulses are applied[6,7,41], and when non-water-suppressed spectroscopy is performed using metabolite cycling[16,17]. Across these studies, total creatine has consistently been reported as the metabolite most strongly affected by saturation transfer effects.

This interpretation is further supported by the absence of corresponding concentration differences in the SPECTRE phantom measurements. Water-mediated magnetisation transfer effects are expected to be strongest in biological tissue, where the presence of many small compartments and restricted molecular mobility facilitate efficient magnetization exchange[7,41,42]. In contrast, the phantom represents a single, large, and homogenous compartment with high molecular mobility, in which saturation transfer effects are expected to be minimal. Consistent with this expectation, no systematic differences in metabolite concentrations were observed between water-suppressed and non-water-suppressed acquisitions in the phantom data.

The larger magnitude and more widespread increases observed in the semi-LASER data compared to the MEGA-PRESS data may reflect sequence-dependent sensitivity to magnetisation transfer effects and macromolecular contributions. The semi-LASER acquisitions were performed with a shorter echo time, resulting in a substantially larger macromolecular signal contribution. Quantification in the presence of a strong macromolecular background is an inherent challenge in MRS, particularly when flexible baselines are used[43], and this challenge may be further compounded in non-water-suppressed acquisitions, as the macromolecular signals themselves have been reported to exhibit saturation transfer effects[41]. The combined influence of water-mediated saturation transfer effects and macromolecular modelling limitations may therefore contribute to the larger apparent changes observed in the semi-LASER acquisitions. Future work may benefit from the use of macromolecular basis sets specifically measured for non-water-suppressed acquisitions.

Conclusion

This work demonstrates that gradient-induced artefactual sidebands in non-water-suppressed MR spectroscopy can be effectively corrected by using the Gradient Impulse Response

Function (GIRF) to predict time-dependent magnetic field perturbations during the FID. The GIRF is measured in a one-time calibration, independently of the spectroscopy acquisition, enabling post-processing correction of the sidebands without requiring sequence modification or specialized hardware. While demonstrated here for two single-voxel-spectroscopy (SVS) sequences at 3T, the approach is, in principle, extendable to other SVS sequences and field strengths, subject to appropriate system calibration.

Data and Code Availability Statement

The data and code used in this work are made available online. Code relating to the measurement and calculation of the Gradient Impulse Response Function (GIRF) is available at https://github.com/jbbacon/GIRF_PE_Python (specific git hash 89ae82a) with data and a permanent record available at https://doi.org/10.5281/zenodo.15350583. Code and data relating to preprocessing, GIRF correction and spectral fitting is available at https://github.com/jbbacon/NWS_Spectroscopy (specific git hash cb309bb) with a permanent record available at https://doi.org/10.5281/zenodo.18262880. Data is provided after initial preprocessing for one representative participant to demonstrate the GIRF correction pipeline, and for all participants prior to spectral fitting.

Acknowledgements

This research was funded by the Wellcome grant [225924/Z/22/Z] and supported by the NIHR Oxford Health Biomedical Research Centre (NIHR203316). The views expressed are those of the authors and not necessarily those of the NIHR or the Department of Health and Social Care. The Centre for Integrative Neuroimaging was supported by core funding from the Wellcome Trust (203139/Z/16/Z and 203139/A/16/Z). JB and PJ acknowledge support from the Vivensa Foundation. PJ also acknowledges support from the NIHR Oxford Biomedical Research Centre (NIHR203311).

This research was funded in whole, or in part, by the Wellcome Trust [Grant number 225924/Z/22/Z]. For the purpose of open access, the author has applied a CC BY public copyright licence to any Author Accepted Manuscript version arising from this submission.

References

1. Nixon TW, McIntyre S, Rothman DL, de Graaf RA. Compensation of gradient-induced magnetic field perturbations. *Journal of Magnetic Resonance*. 2008;192(2):209-217. doi:https://doi.org/10.1016/j.jmr.2008.02.016

2. Dreher W, Leibfritz D. New method for the simultaneous detection of metabolites and water in localized in vivo 1H nuclear magnetic resonance spectroscopy. *Magnetic Resonance in Medicine*. 2005;54(1):190-195. doi:https://doi.org/10.1002/mrm.20549

3. Clayton DB, Elliott MA, Leigh JS, Lenkinski RE. 1H spectroscopy without solvent suppression: Characterization of signal modulations at short echo times. *Journal of Magnetic Resonance*. 2001;153(2):203-209. doi:https://doi.org/10.1006/jmre.2001.2442

4. Chadzynski GL, Klose U. Chemical shift imaging without water suppression at 3 T. *Magnetic Resonance Imaging*. 2010;28(5):669-675. doi:https://doi.org/10.1016/j.mri.2010.01.008

5. Leibfritz D, Dreher W. Magnetization transfer MRS. *NMR in Biomedicine*. 2001;14(2):65-76. doi:https://doi.org/10.1002/nbm.681

6. Dreher W, Norris DG, Leibfritz D. Magnetization transfer affects the proton creatine/phosphocreatine signal intensity: In vivo demonstration in the rat brain. *Magnetic Resonance in Medicine*. 1994;31(1):81-84. doi:https://doi.org/10.1002/mrm.1910310114

7. de Graaf RA, van Kranenburg A, Nicolay K. Off-resonance metabolite magnetization transfer measurements on rat brain in situ. *Magnetic Resonance in Medicine*. 1999;41(6):1136-1144. doi:10.1002/(SICI)1522-2594(199906)41:6%3C1136::AID-MRM9%3E3.0.CO;2-G

8. Deelchand DK, Joers JM, Auerbach EJ, Henry PG. Prospective motion and B0 shim correction for MR spectroscopy in human brain at 7T. *Magnetic Resonance in Medicine*. 2019;82(6):1984-1992. doi:https://doi.org/10.1002/mrm.27886

9. Serrai H, Clayton DB, Senhadji L, Zuo C, Lenkinski RE. Localized proton spectroscopy without water suppression: Removal of gradient induced frequency modulations by modulus signal selection. *Journal of Magnetic Resonance*. 2002;154(1):53-59. doi:https://doi.org/10.1006/jmre.2001.2462

10. Koolschijn RS, Clarke WT, Ip IB, Emir UE, Barron HC. Event-related functional magnetic resonance spectroscopy. *NeuroImage*. 2023;276:120194. doi:https://doi.org/10.1016/j.neuroimage.2023.120194

11. Gonçalves SI, Ligneul C, Shemesh N. Short echo time relaxation-enhanced MR spectroscopy reveals broad downfield resonances. *Magn Reson Med*. 2019;82(4):1266-1277. doi:10.1002/mrm.27806

12. Dong Z. Proton MRS and MRSI of the brain without water suppression. *Progress in Nuclear Magnetic Resonance Spectroscopy*. 2015;86-87:65-79. doi:https://doi.org/10.1016/j.pnmrs.2014.12.001

13. Van Vaals JJ, Bergman AH. Optimization of eddy-current compensation. *Journal of Magnetic Resonance (1969)*. 1990;90(1):52-70. doi:https://doi.org/10.1016/0022-2364(90)90365-G

14. Jensen DJ, Brey WW, Delayre JL, Narayana PA. Reduction of pulsed gradient settling time in the superconducting magnet of a magnetic resonance instrument. *Medical physics*. 1987;14(5):859-862.

15. Dong Z, Dreher W, Leibfritz D. Experimental method to eliminate frequency modulation sidebands in localized in vivo 1H MR spectra acquired without water suppression. *Magn Reson Med*. 2004;51(3):602-606. doi:10.1002/mrm.10716

16. Emir UE, Burns B, Chiew M, Jezzard P, Thomas MA. Non-water-suppressed short-echo-time magnetic resonance spectroscopic imaging using a concentric ring k-space trajectory. *NMR Biomed*. 2017;30(7). doi:10.1002/nbm.3714

17. Deelchand DK, Henry PG. Effect of water suppression and metabolite cycling n quantification of 1H MRS spectra in the human brain at 3 Tesla. *Proceedings of the International Society for Magnetic Resonance in Medicine*. 2020;28(2895).

18. Chadzynski GL, Klose U. Proton CSI without solvent suppression with strongly reduced field gradient related sideband artifacts. *MAGMA*. 2013;26(2):183-192. doi:10.1007/s10334-012-0338-3

19. Tkác I, Starcuk Z, Choi IY, Gruetter R. In vivo 1H NMR spectroscopy of rat brain at 1 ms echo time. *Magn Reson Med*. 1999;41(4):649-656. doi:10.1002/(sici)1522-2594(199904)41:4%3C649::aid-mrm2%3E3.0.co;2-g

20. Ogg RJ, Kingsley PB, Taylor JS. WET, a T1- and B1-insensitive water-suppression method for in vivo localized 1H NMR spectroscopy. *J Magn Reson B*. 1994;104(1):1-10. doi:10.1006/jmrb.1994.1048

21. Haase A, Frahm J, Hänicke W, Matthaei D. 1H NMR chemical shift selective (CHESS) imaging. *Phys Med Biol*. 1985;30(4):341-344. doi:10.1088/0031-9155/30/4/008

22. Klose U. In vivo proton spectroscopy in presence of eddy currents. *Magnetic Resonance in Medicine*. 1990;14(1):26-30. doi:https://doi.org/10.1002/mrm.1910140104

23. Vannesjo SJ, Haeberlin M, Kasper L, Pavan M, Wilm BJ, Barmet C, et al. Gradient system characterization by impulse response measurements with a dynamic field camera. *Magn Reson Med*. 2013;69(2):583-593. doi:10.1002/mrm.24263

24. Lathi BP, Green RA. *Signal Processing and Linear Systems*. Vol 2. Oxford university press Oxford; 1998.

25. Barnett A. Comments on “gradient-induced acoustic and magnetic field fluctuations in a 4T whole-body MR imager”. *Magn Reson Med*. 2001;46(2):207. doi:10.1002/mrm.1179

26. Rizzo Sierra CV, Versluis MJ, Hoogduin JM, Duifhuis HD. Acoustic FMRI noise: linear time-invariant system model. *IEEE Trans Biomed Eng*. 2008;55(9):2115-2123. doi:10.1109/TBME.2008.923112

27. Vannesjo SJ, Graedel NN, Kasper L, Gross S, Busch J, Haeberlin M, et al. Image reconstruction using a gradient impulse response model for trajectory prediction. *Magn Reson Med*. 2016;76(1):45-58. doi:10.1002/mrm.25841

28. Duyn JH, Yang Y, Frank JA, van der Veen JW. Simple correction method for k-space trajectory deviations in MRI. *J Magn Reson*. 1998;132(1):150-153. doi:10.1006/jmre.1998.1396

29. Bacon JB, Jezzard P, Clarke WT. Book of Abstracts ESMRMB 2025 Online 41st Annual Scientific Meeting 8–11 October 2025. *Magnetic Resonance Materials in Physics, Biology and Medicine*. 2025;38(1):684-685. doi:10.1007/s10334-025-01278-8

30. Wu Z, Jaffray A, Vannesjo SJ, Uludağ K, Kasper L. MR System Stability and Quality Control using Gradient Impulse Response Functions (GIRF). *Proceedings of the International Society for Magnetic Resonance in Medicine*. 2022;30(0641).

31. Robison RK, Li Z, Wang D, Ooi MB, Pipe JG. Correction of B(0) eddy current effects in spiral MRI. *Magn Reson Med*. 2019;81(4):2501-2513. doi:10.1002/mrm.27583

32. Rahmer J, Mazurkewitz P, Börnert P, Nielsen T. Rapid acquisition of the 3D MRI gradient impulse response function using a simple phantom measurement. *Magn Reson Med*. 2019;82(6):2146-2159. doi:10.1002/mrm.27902

33. Deelchand DK, Berrington A, Noeske R, Joers JM, Arani A, Gillen J, et al. Across-vendor standardization of semi-LASER for single-voxel MRS at 3T. *NMR Biomed*. 2021;34(5):e4218. doi:10.1002/nbm.4218

34. *The Use of Magnetic Resonance Spectroscopy as a Tool for the Measurement of Bi-Hemispheric Transcranial Electric Stimulation Effects on Primary Motor Cortex Metabolism.*; 2014. doi:10.3791/51631

35. Miller KL, Alfaro-Almagro F, Bangerter NK, Thomas DL, Yacoub E, Xu J, et al. Multimodal population brain imaging in the UK Biobank prospective epidemiological study. *Nat Neurosci*. 2016;19(11):1523-1536. doi:10.1038/nn.4393

36. Clarke WT, Stagg CJ, Jbabdi S. FSL-MRS: An end-to-end spectroscopy analysis package. *Magn Reson Med*. 2021;85(6):2950-2964. doi:10.1002/mrm.28630

37. Near J, Harris AD, Juchem C, Kreis R, Marjańska M, Öz G, et al. Preprocessing, analysis and quantification in single-voxel magnetic resonance spectroscopy: experts' consensus recommendations. *NMR in Biomedicine*. 2021;34(5):e4257. doi:https://doi.org/10.1002/nbm.4257

38. Davies-Jenkins CW, Zöllner HJ, Simicic D, Hui SCN, Song Y, Hupfeld KE, et al. GABA-edited MEGA-PRESS at 3 T: Does a measured macromolecule background improve linear combination modeling? *Magnetic Resonance in Medicine*. 2024;92(4):1348-1362. doi:https://doi.org/10.1002/mrm.30158

39. Mescher M, Merkle H, Kirsch J, Garwood M, Gruetter R. Simultaneous in vivo spectral editing and water suppression. *NMR Biomed*. 1998;11(6):266-272. doi:10.1002/(sici)1099-1492(199810)11:6%3C266::aid-nbm530%3E3.0.co;2-j

40. Wilson M. Adaptive baseline fitting for MR spectroscopy analysis. *Magnetic Resonance in Medicine*. 2021;85(1):13-29. doi:https://doi.org/10.1002/mrm.28385

41. Hoefemann M, Döring A, Fichtner ND, Kreis R. Combining chemical exchange saturation transfer and (1) H magnetic resonance spectroscopy for simultaneous determination of metabolite concentrations and effects of magnetization exchange. *Magn Reson Med*. 2021;85(4):1766-1782. doi:10.1002/mrm.28574

42. Yadav NN, Yang X, Li Y, Li W, Liu G, van Zijl PCM. Detection of dynamic substrate binding using MRI. *Sci Rep*. 2017;7(1):10138. doi:10.1038/s41598-017-10545-1

43. Giapitzakis IA, Borbath T, Murali-Manohar S, Avdievich N, Henning A. Investigation of the influence of macromolecules and spline baseline in the fitting model of human brain spectra at 9.4T. *Magn Reson Med*. 2019;81(2):746-758. doi:10.1002/mrm.27467